Electronic Supplementary Material (ESI) for Journal of Materials Chemistry C.

Electronic Supplementary Information

Exploring Local Electronic Structure and Geometric Arrangement of ALD Zn(O,S) Buffer Layers using X-Ray Absorption Spectroscopy

*Anup L. Dadlani*ǂ,[1] *Orlando Trejo*ǂ,[2] *Shinjita Acharya*ǂ,[2] *Jan Torgersen,*[2] *Ioannis Petousis,*[3] *Dennis Nordlund,*[4] *Ritimukta Sarangi,*[4] *Peter Schindler,*[2] *and Fritz B. Prinz**[2,3]

[1] Department of Chemistry, Stanford University, Stanford, CA 94305

[2] Department of Mechanical Engineering, Stanford University, Stanford, CA 94305, USA

[3] Department of Materials Science and Engineering, Stanford University, Stanford, CA 94305, USA

[4] Stanford Synchrotron Radiation Lightsource, SLAC National Accelerator Laboratory, Menlo Park, CA 94025, USA

ǂ These authors contributed equally to this work

Experimental Methods

Optical reflectivity measurements were performed on a Perkin Elmer Lambda 1050 UV-vis/NIR Spectrophotometer and the reflectance data was graphed in a Tauc plot which yielded band gaps.

AFM was done using JEOL SPM 5200 system where imaging was done in AC mode.

XPS was done using PHI Versa Probe Scanning XPS Microprobe which uses Al (Kα) radiation of 1486 eV in a vacuum environment of $5*10^{-7}$ Torr.

XRD on the samples was performed in a PANalytical X'Pert PRO X-ray diffraction system. The grazing incidence angle omega was set to 0.5° and Cu Kα radiation with a wavelength of 1.540598 Å was used.

ALD of Zn(O,S) films

ALD was employed to deposit the Zn(O,S) and ZnO layers on the TiO_2 anode, due to its self-limiting, layer-by-layer nature. Samples were deposited on TiO_2 nanoparticles because the XANES signal obtained from material deposited on a nanoporous substrate may be enhanced by the high surface area. In addition, TiO_2 nanoparticle substrates are commonly used in solar cell architectures, acting as a transparent conducting oxide. We used this approach to characterize the coordination environment of the Zn(O,S) buffer layer. We analyzed two sets of samples for comparison: various compositions of S in ALD Zn(O,S) films deposited directly on silica and FTO coated with anatase TiO_2 nanoporous (NP) substrates. The samples used for the XANES studies were about 15 mm x 10 mm x 1.5 mm. The substrates were loaded into a customized flow-type ALD system designed for the deposition of Zn(O,S) thin films. The substrate temperature was maintained at 160 °C. Diethylzinc (DEZ), distilled H_2O, and a gas mixture of 3.5% H_2S in N_2 were used as precursors to deposit Zn(O,S). All of the precursors were given a residence time in the reaction chamber of 2 s to ensure their uniform infiltration of the nanoporous TiO_2 film. After each precursor pulse, 45 s were allotted for byproduct evacuation. The ALD materials were deposited sequentially and without breaking vacuum to prevent contamination or surface restructuring due to air exposure.

Because we found that substrate played no effect on the XANES spectra, the XANES spectra were omitted for samples deposited on silica. All samples analyzed had 300 cycles deposited. In each case, Zn(O,S) layers were deposited using 10, 20, and 33% of ALD oxidant pulses being

H_2S. Take for example 33% sample, we did 2 cycles of DEZ/H_2O plus 1 cycle of Zn/H_2S in each super cycle (100 super cycles to form the 300 cycles mentioned in the manuscript).

The quality of the films was checked by a number of techniques. XPS was done to check the stoichiometry (Fig. S1), GIXRD to check crystallinity (Table S3 and Fig. S4), XRR to check film thickness and density (Table S2 and Fig. S3), and AFM to check film morphology and roughness (Fig. S2).

XANES for Sulfur K-edge measurements

At BL 4-3, the samples were set at 45° from the incident x-ray beam and detector. The energy X-ray slits were set at 1 mm x 10 mm. A Passivated Implanted Planar Silicon (PIPS) detector was used to gather the total fluorescence yield (TFY) data. During the S K-edge measurements, the samples and X-ray path were under a He environment.

XANES for Oxygen K-edge measurements

Auger electron yield (AEY) and total electron yield (TEY) spectra were gathered at BL 10-1. To measure the sample drain current for the TEY data, all samples were loaded on the sample stick with carbon tape and were electrically grounded with carbon paste.

XPS measurement

Different oxidant ratios gave different compositions, which were analyzed by XPS of Zn $2p_{3/2}$, S $2p_{3/2}$ and O 1s spectra as shown in Fig.S1. Scanning the survey spectra for these films indicate the presence of surface impurities like carbonates and hydroxide which is well known for ALD films especially deposited at lower temperatures (<200 °C).[1] To accurately quantify the concentration of O in the film, the surface was cleaned using Ar^+ ion sputtering (2kV, 1μA,) 1×10^{-7} Torr) at the rate of 6 nm/min before the scan. We observed that the S content increases as the ratio of H_2S to total oxidant pulses increases. The S concentration with respect to $H_2S/(H_2S+H_2O)$ increases in a manner consistent with findings of Bugot et al.[2] This is due to the replacement of O by S ions induced by adsorbed H_2S, a thermodynamically favorable process as described by Platzer-Björkman et al.[3] However, the mismatch observed here shows that the growth of Zn(O,S) films does not reach surface saturation in each layer.

All the films are slightly Zn rich (52-57%). This is likely because O and S sputter quicker than Zn due to the higher atomic weight of Zn. This leads to a slight overrepresentation of Zn.[4] The binding energies of the three elements does not change much with composition and no trend is observed, tabulated in Table S1. The observations above provided us information on the Zn(O,S) compositions with respect to the $H_2S/(H_2S + H_2O)$ cycles but have also shown us the limitations of XPS.

GIXRD measurement

In an attempt to understand the atomic rearrangement and crystallographic features in the films, GIXRD was performed (Fig. S4), peak positions with corresponding planes are shown in Table S3. ALD ZnO is wurtzite and the ZnS is spahlerite, while varying concentrations of Zn(O,S) fall in between these two reference samples, each exhibiting different levels of crystallinity. Although clearly distorted, the 10% sample most closely resembles ZnO while 20% and 33% more closely resemble ZnS.[3] With increasing S concentration, the diffraction angles decrease. 10% has c/a = 1.62, which is close to the pure ZnO and it presumably still crystallizes in a distorted wurtzite lattice. 20% (S/Zn = 0.361) is not amorphous, contrary to Platzer-Björkman *et al.*[3] which might be a result of different deposition conditions employed. All the stoichiometries are no longer wurtzite or cubic like the reference samples, because the peak shifts are not isotropic.

Simulations

We demonstrate the nature of bonding distortions in Zn(O,S) through multiple-scattering simulations of Zn(O,S) clusters. Theoretical XANES spectra are simulated using the FEFF9 code[5],[6] based on Green's function multiple-scattering theory where the parameters SCF (specifies the radius of the cluster for full multiple scattering during the self-consistency loop) and FMS (computes full multiple scattering within a sphere of radius **r** centered on the absorbing atom) were changed. We first obtained spectral agreement between simulated and experimental wurtzite ZnO and spahlerite ZnS. As a basis for simulating differences observed in the O and S K-edge XANES spectra of the Zn(O,S) samples, structural data was obtained by incorporating varying amounts of S (initally from XPS data, Table S5) into a wurtzite ZnO matrix and then allowing it to relax using Density Functional Theory (DFT)[7] calculations in VASP with certain constraints provided from XRD data. For the DFT calculations we used PAW pseudopotentials[8,9] and the PBE exchange-correlation functional[10,11] with an energy cut-off of 520 eV. We started with (1) the pure ZnO structure from the International Crystallographic Database (ICSD)[12] with code 163380, and created 3 additional supercells (2) 2x1x1 (3) 2x2x1 and (4) 2x2x2. In each case we replaced one O atom with S to simulate the different compositions. For each supercell we used the following k-point grids respectively: (1) 11x11x8, (2) 6x11x8, (3) 6x6x8 and (4) 6x6x4. In Table S4 all the structures obtained by DFT and used as input files in FEFF are shown. We noticed that lower concentrations of S in calculated structures were in better agreement with experimental samples. This is likely due to the large DOS surrounding S atoms, hence the inclusion of S atoms has a dramatic effect on calculated XANES spectra as explained by Sipr.[13] An example of two inputs we used for XANES simulations are shown in Fig. S5. Fig. S5a shows pure ZnO wurzite lattice with an α = 90° and b = 3.29 Å. The input used to simulate 20% which contained 12.5% S is shown in Fig. S5b, where the angle α has been distorted from 90° in pure wurzite ZnO to 84.47° and lattice constant b has changed from 3.29 Å in pure wurtzite ZnO to 3.39 Å, pointing to lattice expansion with S incorporation. The distribution of charges for the atoms in Zn(O,S) was calculated by Bader charge analysis (Table S6). It is known that ZnO is one of the most covalent monoxides.[14] The value for ZnO shows that O has a charge of -1.2265, which supports that ZnO is quite covalent. As the S content increases, it is observed that the Zn gets more ionic and the O gets more covalent, except in the case of the 12.5% S containing sample. One particular Zn atom is more ionic than the rest and that makes the average Zn ionicity greater in this structure than the other stoiciometries. This is caused by a S-O bond that exists in the structure that may or may not exist in reality.

LDOS

The LDOS was calculated for all the simulated XANES spectra that has been shown, using FEFF. The partial density of states (pDOS) were then properly aligned to the Fermi level by shifting the total density of states (tDOS) so that the onset of the band gap was at 0 eV. Next the experimental curves were aligned by shifting it so that the highest intensity was in line with the highest intensity of the pDOS of the absorbing anion. Fig.S6 shows the pDOS curves placed underneath the pertinent experimental curves. Fig.S6a, O K edge of 10%, the calculations reveal that O 2p and S 3p are the main contributors to the onset of the absorption spectrum. Looking at Fig.S6b, the S K edge, shows that S 3p and Zn 4s and O 2p are the greater contributors at the onset. Fig.S6c, O K edge of 33%, it is seen that O 2p, S 3p and Zn 4s are the major contributors of the hybridized orbitals in the conduction band close to the onset. Fig.S6d, S K edge of 33% has contributions from S 3p, O 2p, and Zn 4s at the main absorption peak.

UV-Vis measurement

The band gap is plotted in Fig. S7. The band gap was measured using diffuse reflectance on samples made on silicon wafer, because those were the substrates used for XAS studies. The reflectance data was then made into a Tauc plot, from which the band gap was extracted. The band gap for ZnS is 3.18 eV, whereas in literature it is 3.55 eV.[3] To verify the band gap value of our ZnS, we deposited it on a quartz wafer and obtained a band gap of 3.5 eV from transmittance data. Hence, the values obtained are not to be taken as absolutes but are meaningful in terms of the trend they reveal. ZnO has a lower band gap of 2.5 eV. The lowest band gaps were actually measured in the Zn(O,S) 10% and Zn(O,S) 20% samples and Zn(O,S) 33%, same as in literature.[3] The 20% sample, which according to XPS is nearly 50-50 in S and O content had the lowest band gap, which is consistent with Sharbati et. al.[15] The Zn(O,S) 33% had a band gap equivalent to ZnO, indicating that one can tune carrier concentration and still maintain a band gap of ZnO if that is desired.

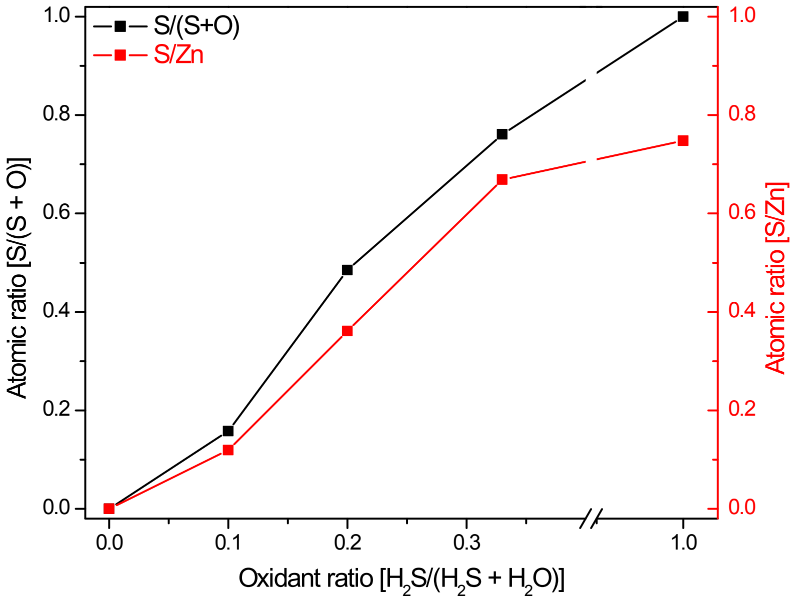

Fig. S1. S/(S+O) (black squares) and S/Zn (red squares) ratio determined as a function of $H_2S/(H_2S + H_2O)$ oxidant pulses by XPS high resolution scans after 6 seconds of sputtering (300 cycles, Si <100>, 160°C deposition temperature). With increasing ratio of H_2S to oxidant pulses, S to total oxidant content increases. All samples are slightly zinc rich, which may be due to faster sputter rates of the lighter elements O and S.[4]

TABLE S1. Properties of ALD Zn(O,S) films deposited (300 cycles, Si <100>, 160 °C). Binding energies obtained for selected energies (high resolution XPS, after 6 s sputtering). Samples are labeled as follows – 0 (ZnO), 10, 20, 33, and 100 (ZnS) % of H_2S pulses to total oxidant pulses.

Thick films	ZnO	10%	20%	33%	ZnS
	BE (eV)	BE (eV)	BE (eV)	BE (eV)	BE (eV)
Zn $2p_{3/2}$	1022.0	1022.2	1022.0	1021.8	1022.2
S $2p_{3/2}$		162.2	162.0	161.8	162.0
O 1s	531.0	530.8	530.4	530.4	

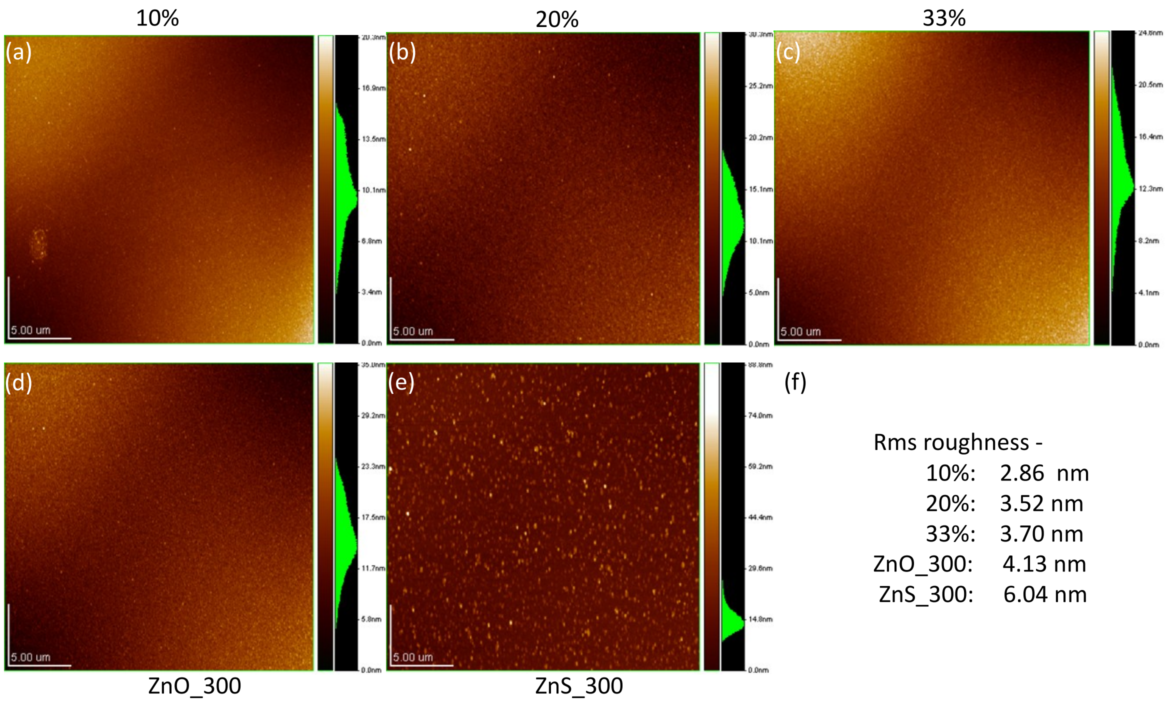

Rms roughness -

10%:	2.86 nm
20%:	3.52 nm
33%:	3.70 nm
ZnO_300:	4.13 nm
ZnS_300:	6.04 nm

Fig. S2: AFM of ALD films (300 cycles) deposited on silicon and imaged in acoustic mode. Each image is a scan of 25 x 25 um^2. Scale bar is 5 µm for all images. (a) 10% (b) 20% (c) 33% (d) reference sample, 300 cycles of ALD ZnO, and (e) reference sample SZnS_300. (f) The root mean square (RMS) roughness of each of the samples is given, where ZnS is roughest. The RMS roughness was obtained on several 25 x 25 um^2 areas for each sample and averaged.

TABLE S2. Density and thickness values obtained by fits from XRR.

Sample	Density (g/cm^3)	Thickness (nm)
ZnO_300	4.90	58.4
10%_300	4.30	58.4
20%_160	3.73	27.9
33%_300	3.60	50.9
ZnS_300	3.55	33.9

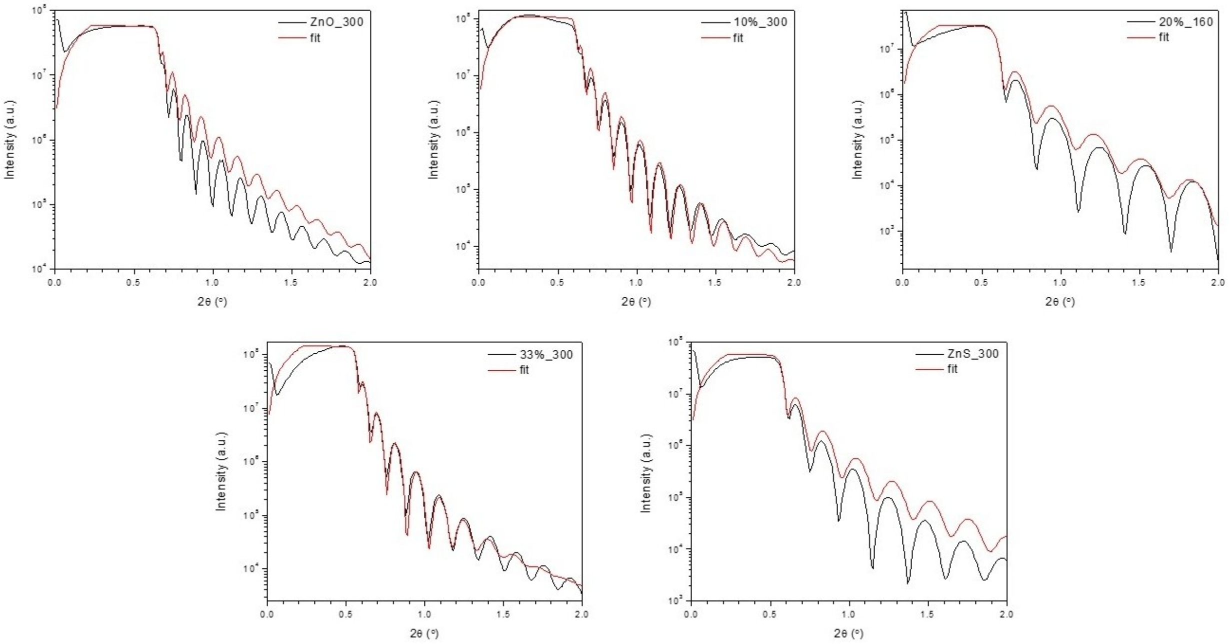

Fig. S3: XRR spectra along with fits from which the density and thickness values were obtained and tabulated in Table S2. The number following the sample name is the number of total cycles.

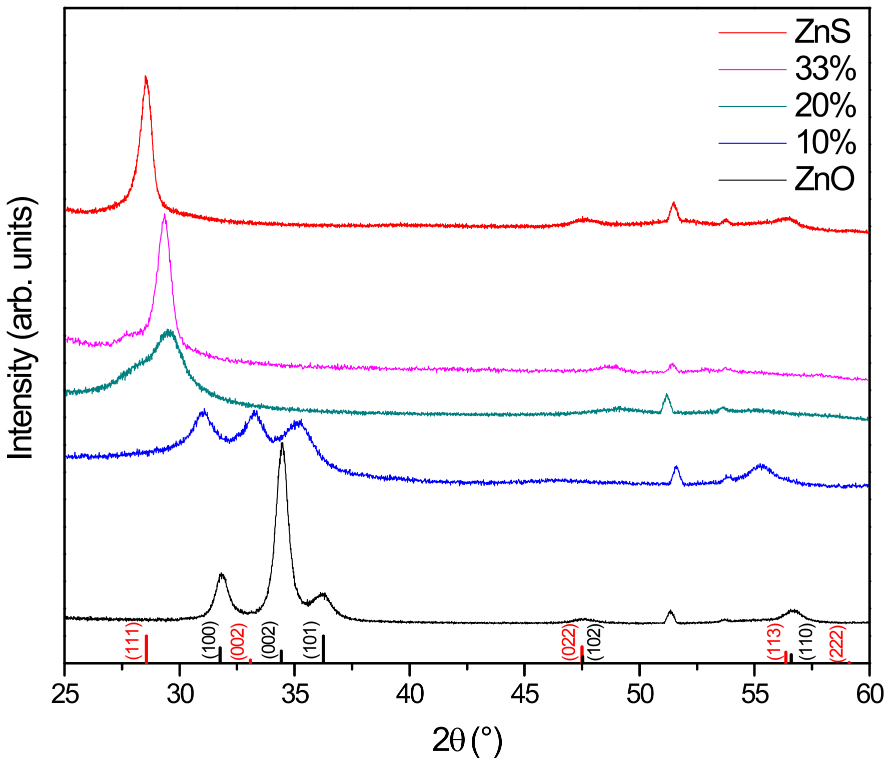

Fig. S4. Grazing incidence diffractograms of Zn(O,S) films (160 °C, Si <100>, 300 cycles) – starting from bottom ZnO, 10%, 20%, 33%, and ZnS films.

TABLE S3. Diffraction planes as measured by grazing incidence x-ray diffraction (GIXRD). ZnO wurtzite film has planes (100), (002), (101), (102), and (110), while ZnS films show peaks of planes (111), (022), and (113). Samples are labeled as follows – 0 (ZnO), 10, 20, 33, and 100 (ZnS) % of H_2S pulses to total oxidant pulses.

	ZnO	10%	20%	33%	ZnS
XRD peak positions (°, 2Θ)			29.51	29.35	28.51 (111)
	31.81 (100)	31.09			
	34.46 (002)	33.26			
	36.22 (101)	35.29			
	47.59 (102)		49.08	48.68	47.51 (022)
	56.65 (110)	55.24			56.24 (113)

TABLE S4: Clusters obtained from DFT and used as input files in FEFF to simulate the experimental samples.

	ZnO	10%	20%	33%	ZnS
a (Å)	3.289	6.644	6.647	7.329	3.854
b (Å)	3.289	6.645	3.396	3.749	3.854
c (Å)	3.289	10.74	11.077	6.269	3.854
α (°)	90	89.994	84.467	89.978	60
β (°)	90	89.998	89.223	103.734	60
γ (°)	119.99	120.004	120.282	120.783	60

TABLE S5: Clusters obtained from DFT and initially used as input files in FEFF to simulate the experimental samples based off of XPS analysis. These structures did not match the experimental XANES spectra.

	50%	75%
a (Å)	3.617	6.852
b (Å)	3.617	3.428
c (Å)	5.790	5.548
α (°)	90	90.023
β (°)	90	89.653
γ (°)	119.999	119.983

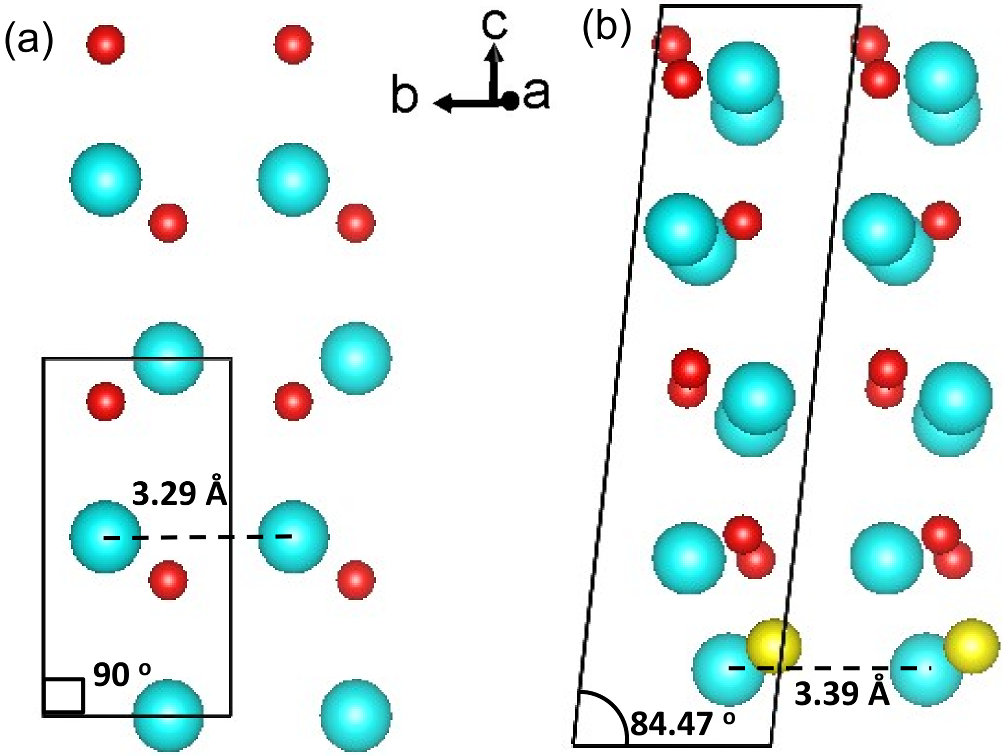

Fig. S5: Clusters (viewed looking down at bc plane) used as inputs for XANES simulations done in FEFF. Color scheme for atoms is as follows - Zinc (aqua), O (red), and S (yellow). (a) Pure wurtzite ZnO cluster showing α = 90° and b = 3.29 Å. (b) ZnO matrix with 12.5% S incorporated to simulate 20% showing α = 84.47° and b = 3.39 Å.

TABLE S6: Bader charge analysis carried out in VASP on structures used for XANES simulations.

	Charge/atom		
Sample	Zn	O	S
ZnO	1.2265	-1.2265	
1S:15O	1.1944	-1.2134	-0.9087
1S:7O	1.0339	-1.1855	0.0278
1S:3O	1.0726	-1.1977	-0.6972
ZnS	0.8529		-0.8529

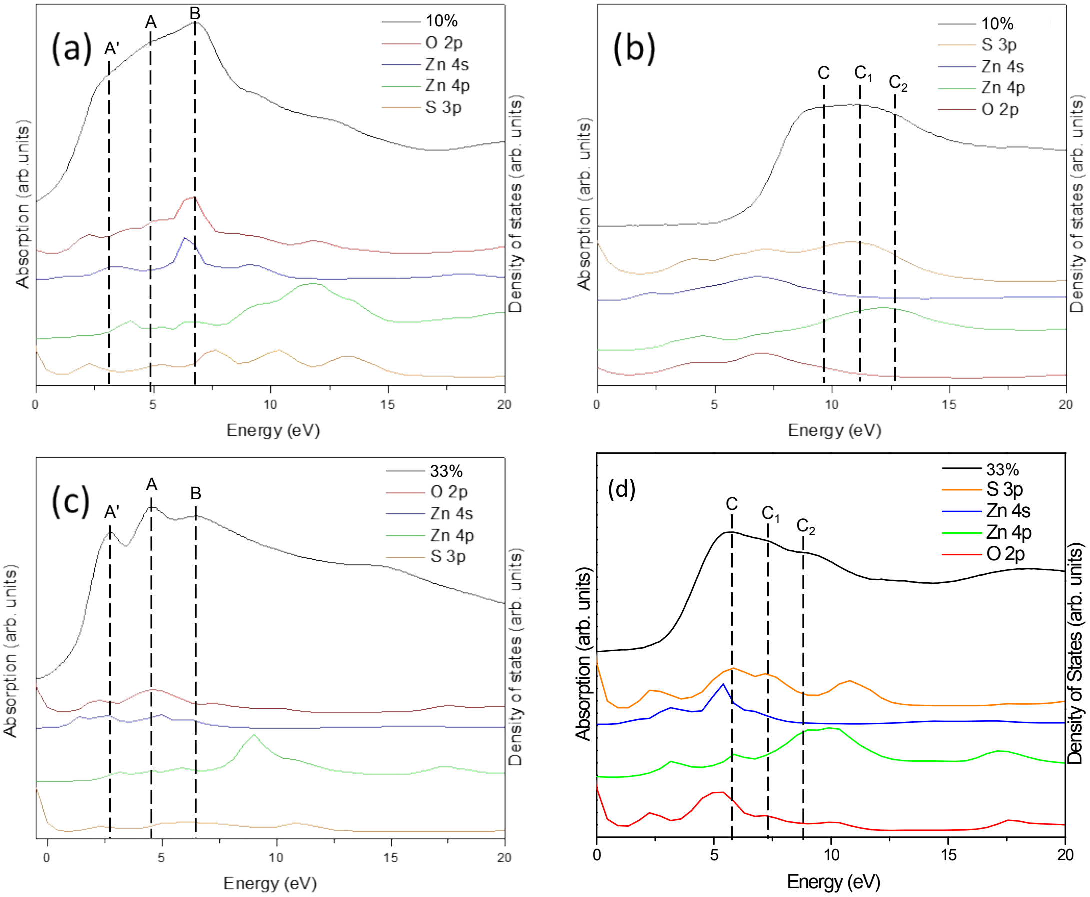

Fig. S6: Calculations of the partial density of states (pDOS) calculated using FEFF and aligned to Fermi level where the relevant experimental O and S K-edge spectra have been shifted so that maximum intensity of absorbing anion matches maximum intensity of empirical spectra. (a) 10%, showing that O 2p, Zn 4s, Zn 4p, and S 3p contribute to the conduction band of Zn(O,S) 10%. There is decent overlap of O 2p and S 3p near the early part of spectrum. (b) pDOS underneath 10% S K edge XANES spectrum showing contributions from S 3p Zn 4sp and O 2p (especially near the main edge). (c) 33% which shows strongest contribution from O 2p, S 3p and Zn 4s at the beginning of spectrum. (d) 33%, under S K-edge spectrum showing strong contributions from S 3p, Zn 4sp, and O 2p to the near edge.

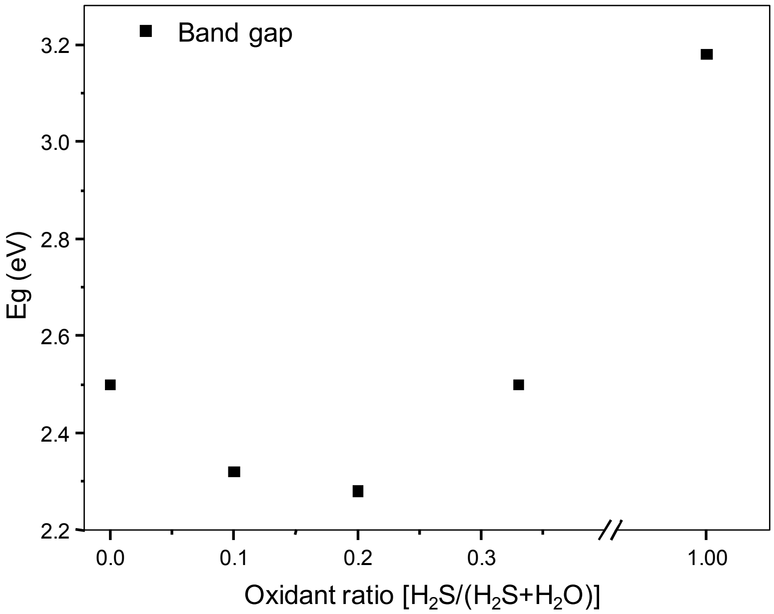

Fig. S7: Band gaps extracted from Tauc plots generated by reflectance data acquired on samples (300 cycles) deposited on silicon as a function of H_2S/(total oxidant pulses).

TABLE S7: Relative band onset offsets with respect to the reference samples obtained from the XANES derivative plot shown in the main paper Figure 5.

Sample	**Relative band offset with respect to ZnO**
10%	+ 0.19 eV
20%	+ 0.19 eV
33%	+ 0.07 eV

Sample	**Relative band offset with respect to ZnS**
10%	- 0.90 eV
20%	- 0.90 eV
33%	- 0.70 eV

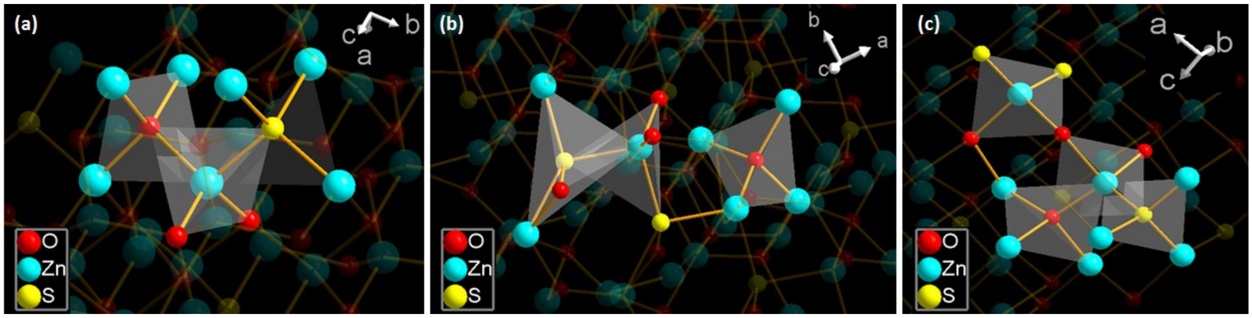

Fig. S8. Moieties present in the different stoichiometries of Zn(O,S) structures that were calculated from VASP and were used in simulating XANES and DOS spectra. (a) 1S:15O was determined to be the best match to the 10% sample (b) 1S:7O was determined to be the best match to the 20% sample and (c) 1S:3O was determined to be the best match to the 33% sample. It is observed that with increasing S concentration, the number of S atoms present in the tetrahedrons increases. Interestingly the 1S:7O shows the existence of a S – O bond which may or may not exist in the actual films. The films are not entirely representative of our films but exhibit trends that are consistent with our findings.

References

1 S. K. Kim, S. W. Lee, C. S. Hwang, Y.-S. Min, J. Y. Won and J. Jeong, *J. Electrochem. Soc.*, 2006, **153**, F69.

2 C. Bugot, N. Schneider, M. Jubault, D. Lincot and F. Donsanti, *J. Vac. Sci. Technol. A*, 2015, **33**, 01A151.

3 C. Platzer-Bjorkman, T. Torndahl, D. Abou-Ras, J. Malmstrom, J. Kessler and L. Stolt, *J. Appl. Phys.*, 2006, **100**, 44506.

4 Y.-S. Min, C.-J. An, S.-K. Kim, J.-W. Song and C.-S. Hwang, *Bull. Korean Chem. Soc.*, 2010, **31**, 2503–2508.

5 J. J. Rehr, J. J. Kas, F. D. Vila, M. P. Prange and K. Jorissen, *Phys. Chem. Chem. Phys.*, 2010, **12**, 5503–5513.

6 J. J. Rehr, J. J. Kas, M. P. Prange, A. P. Sorini, Y. Takimoto and F. Vila, *Comptes Rendus Phys.*, 2009, **10**, 548–559.

7 W. Kohn and L. J. Sham, *Phys. Rev.*, 1965, **140**, A1133–A1138.

8 P. E. Blöchl, *Phys. Rev. B*, 1994, **50**, 17953–17979.

9 G. Kresse and D. Joubert, *Phys. Rev. B*, 1999, **59**, 1758–1775.

10 J. P. Perdew, K. Burke and M. Ernzerhof, *Phys. Rev. Lett.*, 1996, **77**, 3865–3868.

11 J. P. Perdew, K. Burke and M. Ernzerhof, *Phys. Rev. Lett.*, 1997, **78**, 1396.

12 S. Cui, W. Feng, H. Hu, Z. Feng and Y. Wang, *J. Alloys Compd.*, 2009, **476**, 306–310.

13 O. Sipr, *J. Phys. Condens. Matter*, 2001, **13**, 4291.

14 P. Li, Y. Wang and I.-W. Chen, *Ferroelectrics*, 1994, **158**, 229–234.

15 S. Sharbati and J. R. Sites, *Photovoltaics, IEEE J.*, 2014, 4, 697–702.